aerospace

MDPI

Article

Deployment of Solar Sails by Joule Effect: Thermal Analysis and Experimental Results

Gianluigi Bovesecchi †, Sandra Corasaniti †, Girolamo Costanza *,†, Fabrizio Paolo Piferi † and Maria Elisa Tata †

Industrial Engineering Department, University of Rome Tor Vergata, Via del Politecnico 1, 00133 Rome, Italy; gianluigi.bovesecchi@uniroma2.it (G.B.); sandra.corasaniti@uniroma2.it (S.C.); fabriziopaolo.piferi@gmail.com (F.P.P.); elisa.tata@uniroma2.it (M.E.T.)

* Correspondence: costanza@ing.uniroma2.it; Tel.: +39-06-72597185

† These authors contributed equally to this work.

Received: 26 November 2020; Accepted: 15 December 2020; Published: 16 December 2020

Abstract: Space vehicles may be propelled by solar sails exploiting the radiation pressure coming from the sun and applied on their surfaces. This work deals with the adoption of Nickel-Titanium Shape Memory Alloy (SMA) elements in the sail deployment mechanism activated by the Joule Effect, i.e., using the same SMA elements as a resistance within suitable designed electrical circuits. Mathematical models were analyzed for the thermal analysis by implementing algorithms for the evaluation of the temperature trend depending on the design parameters. Several solar sail prototypes were built up and tested with different number, size, and arrangement of the SMA elements, as well as the type of the selected electrical circuit. The main parameters were discussed in the tested configurations and advantages discussed as well.

Keywords: solar sail; aerospace; propulsion; mechanical systems; shape memory alloys; joule effect; thermal analysis

1. Introduction

The working principle of solar sails is based on the impingement of solar radiation photons on the sail surface [1]. In this way the solar radiation pressure can be employed to propel spacecrafts [2,3]. This force can be maximized in the presence of a highly reflective surface and low weight [4]. Since small values of radiation pressure are reached in the solar system, in the order of μPa for the planets close to the Sun, it is necessary to design sails with quite large surfaces in order to exploit this propulsion system. Objects of similar size cannot be transported into the space in the deployed form. Consequently it is necessary to foresee the folding and the packaging so that these, after being stowed inside satellites and then launched into orbit, can properly be deployed once reached their operational position [5]. The employed materials must therefore ensure both handling and strength. Tearing or lacerations during the entire operational life of the sail are not allowed. The application of a low density metallic reflective film [6,7] on the surface must also be possible. The adhesion, on the other side, of a material with a high thermal conductivity must also be allowed so that the heat absorbed by the structure can be quickly disposed of, without increasing temperature excessively. At the same time, to convert the driving force associated with the radiation pressure into a satisfying acceleration, it is advisable to ensure a suitable inclination of the sail with respect to the incident radiation and to reduce as more as possible its overall mass. It is, therefore, clear that lightweight mechanisms capable of allowing its deployment should be provided on each structure; from this perspective, it was thought to use shape memory alloys, instead of the more complex electromechanical devices [8,9] which were used in earlier experiments, such as Mariner 10 (NASA, 1973) [10], ODISSEE (DLR, ESA, NASA, 1999) [11], IKAROS

(JAXA, 2010) [2,12], Nanosail-D2 (NASA, 2010) [13], Lightsail 1–2 (Planetary Society, 2009–2018) [14]. Spinning sail blade technologies were proposed by MacNeal [15] and Burton [16].

In the proposed solution the active Ni-Ti SMA elements, in the form of ribbons applied on each folding, have the purpose to exert a sufficient force for the sail deployment. Many studies by the authors were already carried out involving a self-deploying system based on NiTi SMA self-activated by solar irradiation [17–19]. A deeper comprehension, of the SMA in general [20] and of the shape memory recovery in particular [21–23], can be found in previous works, some of them regarding solar sails [24–26]. Shape memory alloys are able to recover a preset shape just heating them at temperature higher than the critical transformation temperature (typically in the range 65–95 °C). One of the main problems, still open, is the inability to pilot the gradual opening of the sail for perfect positioning with respect to the sun. In the scenario presented in [24] some visible lamps were employed by the authors to simulate the solar radiation, allowing the full self-deployment of the sail in the lab experiments. In the second part of this work a gradual deployment system based on the activation of the SMA elements by Joule Effect, inserted in a small-scale prototype of the sail, was built up and tested. Different configurations, electrical circuits and number of folding were compared.

2. Materials

The sail prototype described in this work was built up with thin commercial aluminum film (12 m thickness, 2700 kg/m^3 density) (Figure 1 left), and better results could be achieved employing thinner aluminum. The sail sub-layer was covered by thin films (2.5 m) of adhesive Kapton (1400 kg/m^3 density) (Figure 1 right).

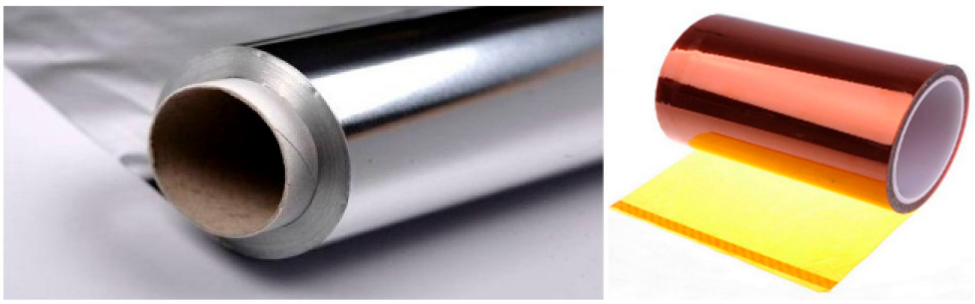

Figure 1. (**left**) commercial aluminum film; (**right**) adhesive Kapton.

Aluminum was selected for the high reflectivity in the whole solar radiation spectrum and Kapton because is chemically inert, shows a high mechanical strength subjected to sunlight radiation and maintains stable its physical and chemical properties also at relatively high temperature. For the active elements, Nitinol SMA (M-alloy produced by Memory Metalle GmbH, Am Kesselhaus 5, 79576 Weil am Rhein, Germany) oxidized wires with a diameter of 0.5 and 0.8 mm were used after rolling to a rectangular cross-section of about 2 × 0.1 mm and 5 × 0.1 mm respectively. SMA are smart materials that can recover the pre-set shape just by heating above the critical transformation temperature. The wires were rolled to obtain ribbons of rectangular cross-section and then sectioned. To set the shape, a particular thermal treatment, called shape-setting, was adopted. It consists of heating up to 500 °C while the SMA ribbon is kept constrained, maintaining at this temperature for 5 min, and finally quenching in cold water. After this treatment, bent in cold conditions (room temperature or lower), the ribbon can recover the preset straight shape just upon heating above the activation temperature (75 °C). For the electrical connection heat-shrink sheaths (Figure 2), electric wires of 0.14 mm^2 (cross-section) and tin brazing were used.

Figure 2. Heat-shrink sheaths for wire connections.

3. Thermal Analysis: Mathematical Models

In a first approach, for the estimation of the electric power required for the activation of the SMA, a lumped system analysis was carried out and a single SMA ribbon in air was analyzed. The element had a rectangular cross-section and it was arranged horizontally with respect to the major sides. Under the hypothesis of thermal homogeneity, the conductive heat exchange that occurs in the junction edges between the ribbon and the electric wires was neglected. The heat fluxes on the ribbon due to the Joule Effect, to the convective and radiative exchange were considered. The solution of the differential heat exchange (Equation (1)) was carried out using the Explicit Euler Method.

$$mc\frac{dT}{dt} = VI - h(T)\cdot A\cdot(T - T_{amb}) - \sigma\epsilon A\left(T^4 - T_{amb}^4\right) \quad (1)$$

Figure 3 shows the time-temperature graph for different applied voltages. It can be noticed that to obtain the complete shape recovery of the ribbon (A_f = 75 °C), 1 V (1.45 A) was not enough. With 1.5 V applied opening times were estimated in about 6.2 s. The range 1.3–2.1 V (i.e., 1.9–3.0 A) allowed a short activation time without excessive temperature increase. The experimental results carried out in the laboratory were found to be in good agreement with the mathematical model chosen.

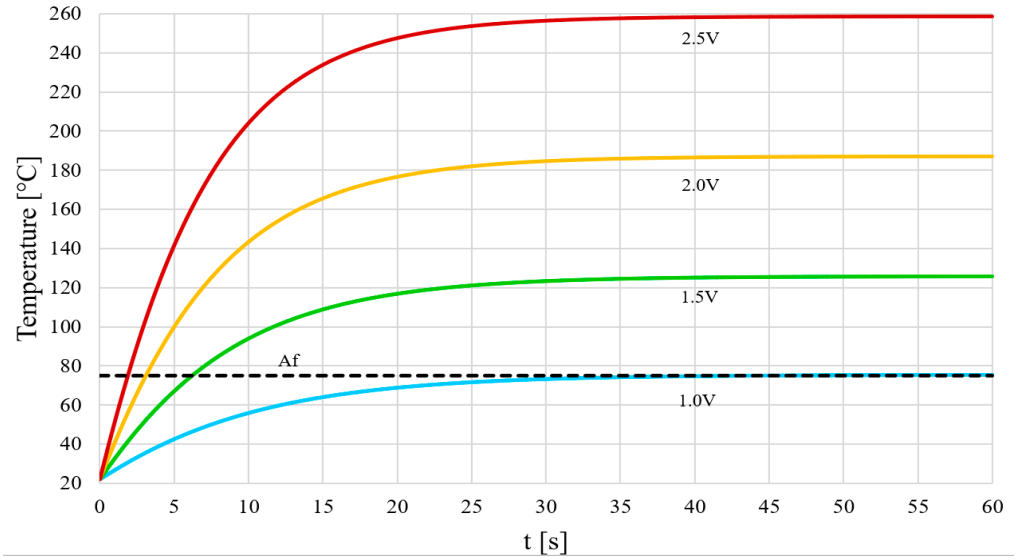

Figure 3. Temperature-Time graph for SMA element in air with different applied voltages.

In a deeper approach, heat transfer between the SMA ribbon (placed between Aluminum and Kapton sheets), and the faces in contact with the Kapton and Aluminum were examined (Equation (2)). A two–dimensional analysis (Fourier equation) was solved, as the thickness of the ribbon was very small. The initial condition (t = 0) was fixed at 20 °C for the whole analyzed domain (0.1 × 0.1 m^2),

while the boundary condition was T (x, 0) = 100 °C (Figure 4). Temperature fields are reported in Figure 4 for different times: for Kapton after 10 min (top) and 10 h (bottom) while for aluminum after 20 s (top) and 30 s (bottom). It can be noticed that the heat conduction in the Kapton (Figure 4 left) is lower than in the Aluminum (Figure 4 right). For the short activation time (a few seconds) the temperature change does not reach areas too far from the SMA ribbon.

$$\frac{\partial T}{\partial t} = \alpha\left(\frac{\partial^2 T}{\partial x^2} + \frac{\partial^2 T}{\partial y^2}\right) \tag{2}$$

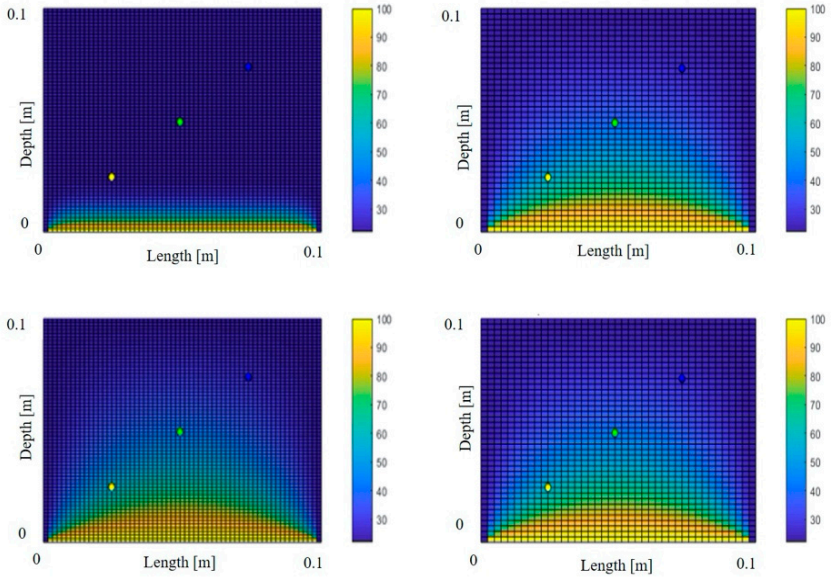

Figure 4. Temperature fields for Kapton® (**left**) and Al (**right**): in the bottom part, steady state graphs; on the top, transient state analysis.

In the third step analysis, the solar sail in a space environment was considered. The main difference is the absence of gravity, which makes negligible the convective heat transfer. Furthermore, the temperature in the space, totally different from the ambient temperature on the earth, affects the heat flux exchanged by irradiation; at last, the solar radiation impacting directly on the solar sail must be taken into account. Therefore, considering the just mentioned contributions to the heat transfer, a lumped system analysis was carried out (Equation (3)) where $I_{o\beta}$ is the real solar irradiance on the sail at the distance Earth-sun and A is the surface of the sail. The SMA ribbon is considered in the middle between a layer of Aluminum and one of Kapton.

$$\rho v c \frac{dT}{dt} = VI + I_{o\beta}A - \sigma A\left(T^4 - T_{amb}^4\right) \tag{3}$$

Figure 5 shows the time-temperature graph for different applied voltages in the space environment the activation time is longer, about 27 s with 1.5 V instead of 6.2 s on the Earth, due to the lower starting temperature and the greater heat exchange by radiation. It is also evident that there is no voltage threshold below which it is not possible to obtain the solar sail deployment.

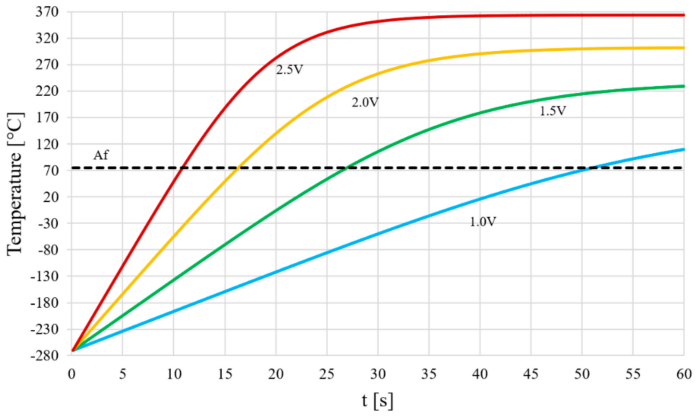

Figure 5. Temperature-Time graph for SMA element in the space environment with different applied voltages.

4. Experimental Results

Some sail prototypes triangular-shaped (300/400 mm base, 150/200 mm height in the deployed conditions) were manufactured in different configurations. A suitable electrical circuit, in which the SMA elements were used as resistances, was therefore made so that the SMA elements can be activated reaching the critical transformation temperature by Joule effect. Some models were designed with different geometric dimensions, number, length, section and arrangement of the SMA elements on the sail, as well as for the different electrical circuits and the number of foldings.

In the first configuration, the circuit provided one SMA element (length 2.5 cm) in series with power supply and with two branches in parallel, each containing five elements connected in series each other (Figure 6a). Between the first and second configurations (surface 225 cm^2, Figure 7), the differences are only in the length of electrical connections (longer in configuration 1), each of them containing 11 SMA elements of the same dimensions (width 1.63 mm, thickness 0.23 mm).

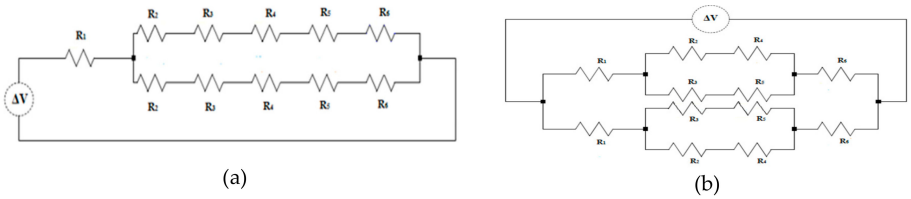

Figure 6. Scheme of the electrical circuits adopted in configurations 1, 2, 4 (**a**) and configuration 3 (**b**).

In the third configuration (Figure 7) the sail size increased (400 cm^2) as well the number of foldings. Two parallel branches were connected in series (Figure 6b) to four other branches, in parallel two by two, each containing two SMA elements in series, and connected in series to the last two resistances of 2.5 cm length in parallel each other (see Figure 6b).

In the fourth configuration (Figure 6) the electrical circuit was simpler, similar to the first and second cases, reducing the number of parallel branches. The number of the elements was increased to 15 to "strengthen" the corners that once folded, should were opened simultaneously. Finally, to improve sail planarity it was decided to employ 0.8 mm SMA and 0.5 mm SMA, dimensions of the wire before rolling, to increase each resistance and consequently the maximum temperature in order to allow a correct opening sequence. In configuration 5 (Figure 7) the circuit remained analogous to the previous and to improve planarity a fourth folding was added. The total surface was kept 400 cm^2. Figure 8 shows an example of a sail opening sequence.

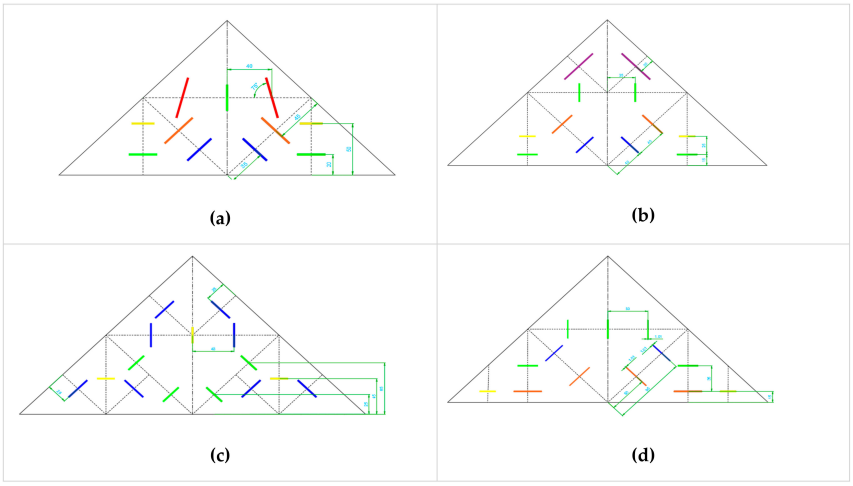

Figure 7. Sail prototypes configurations with SMA elements: (**a**) configurations 1 and 2; (**b**) configuration 3; (**c**) configuration 4; and (**d**) configurations 5 and 6. Length of SMA elements: 5 cm, 4 cm, 3.5 cm, 3 cm, 2.5 cm, 2 cm.

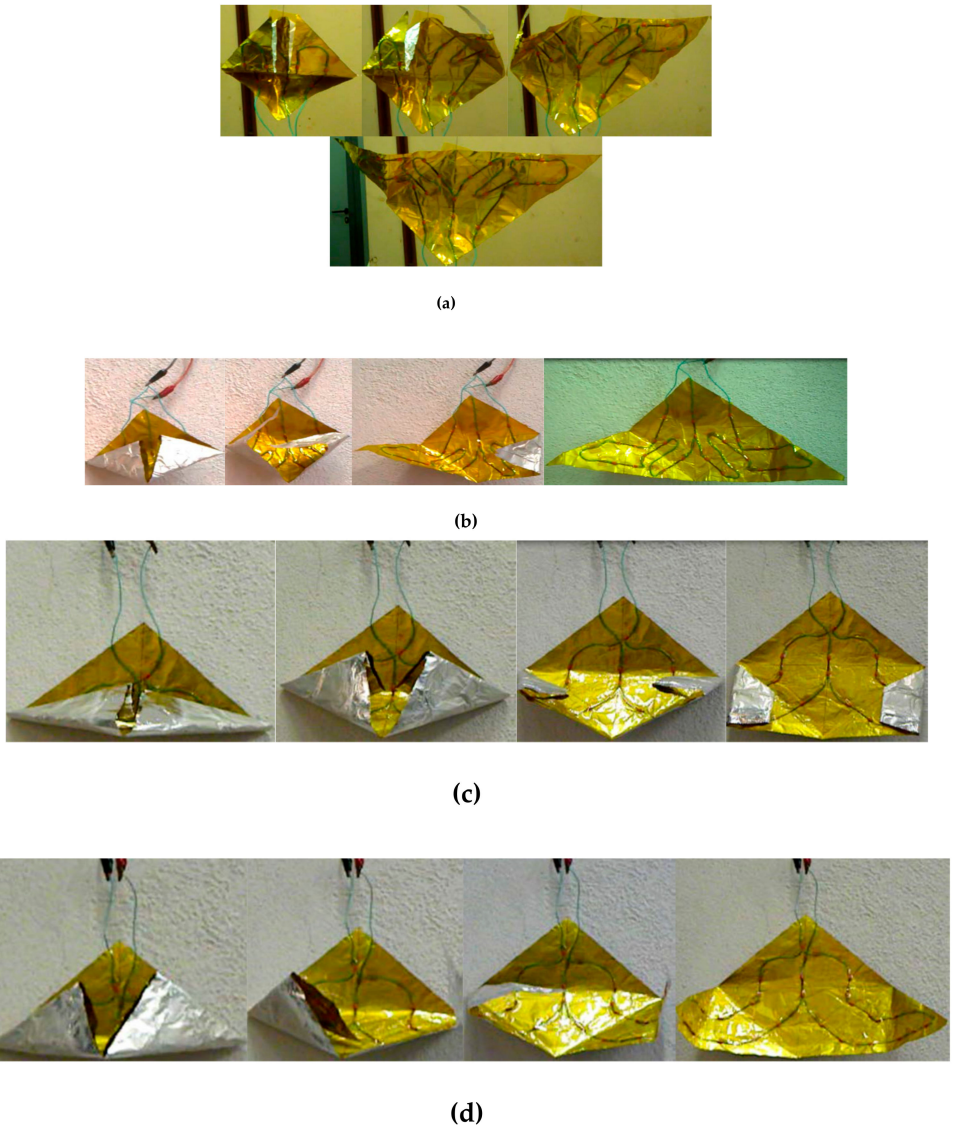

Figure 8. Sail prototypes: deployment sequence of configuration 1 (**a**), 2 (**b**), 5 (**c**), and 6 (**d**).

5. Discussion

In Table 1 the main features of the sail configurations are reported. The optimization of the electrical connections allowed to reduce the opening times from 95 s (configuration 1) to 40 s (configuration 2) maintaining the number of foldings (3) and the surface reduction (75%) of the sail. As a consequence, the electrical junction surface is reduced from 10.1% to 8.2%.

Table 1. Main features of the different sail configurations.

Configuration	Number of Foldings	Surface Reduction	Electrical Junction Surface	Number of SMA Elements	Opening Times	Current Voltage
1	3	75%	10.1%	11	95 s	5 A 2.8 V
2	3	75%	8.2%	11	40 s	5 A 2.6 V
3	4	93%	8.1%	12	75 s	7.5 A 3.0 V
4	4	93%	5.5%	15	55 s	6.0 A 3.6 V
5	4	75%	5.5%	13	100 s	3.1 A 2.2 V
6	3	75%	5.5%	13	70 s	3.1 A 2.5 V

In the configuration 3, with four foldings and 93% surface reduction, 75 s were required for the deployment of the sail while in configuration 4, with four foldings and 93% surface reduction, a shorter opening time, 55 s, was measured. Despite a greater number of active elements adopted in configuration 4 (15 vs. 12), the electrical junction surface is lower (5.5% vs. 8.1%), due to the choice of a single parallel scheme adopted for the electrical circuit instead of the double parallel circuit (configuration 3).

In the configurations 5 and 6 a simpler electrical scheme, similar to that one in Figure 6a, with six resistances instead of five in each branch of the parallel was adopted. The number of SMA elements is 13 for both obtained by rolling SMA wires 0.5 and 0.8 mm diameters for configuration 5 while only 0.5 mm wires were employed for the active elements in configuration 6. The placement of the SMA elements was selected to guarantee better planarity than configuration 4. As shown in Table 1 lower voltage and current were necessary. Opening times of 100 s and 70 s were measured respectively in configurations 5 and 6: shorter time is due to the lower foldings (3 vs. 4) and reduced cross-section in configuration 6 because only 0.5 mm wires were employed for the manufacturing of the SMA active elements.

6. Conclusions

Fine results were obtained from the first two configurations (5 A and 40 ÷ 95 s opening times, see Table 1) with high electrical junction surface (10.1 and 8.2% respectively.) The configurations 3 and 4 allowed a greater reduction surface (93% instead of 75%) and a reduced electrical junction surface (8.1 and 5.5% respectively) but a higher electrical power was necessary for the full activation requiring 75 and 55 s. In configuration 4 a simpler electrical circuit was adopted. The excessive number of folding (configurations 3 and 4) does not allow a satisfactory sail's planarity. Best results were obtained with the last two configurations. In configuration 6 the sail was able to unfold perfectly in about 75 s thanks to the lower number of foldings, simplicity of the electrical circuit, the use of a smaller section of the SMA active elements and reduced power consumption. One of the most important issue concerns the weight increase of the structure to be launched: the surface of the electric wires occupies about 5.5% of the entire sail, and in terms of weight it is about 28% of the total load of the sail. The proposed activation method for the SMA employing current flow can be useful to overcome the problem of the

activation temperature not reached in all SMA elements on the sail due to the low thermal conductivity of the Kapton. More in general, another advantage of the electrical activated SMA elements is the possibility to establish a priori a certain opening sequence by designing the electrical circuit to be used (i.e., deciding which resistances to have in series and which in parallel) and by varying the geometric dimensions of the SMA elements on the sail. Furthermore, it is possible to start the unfolding process at any distance from the Sun and also outside the bright cone. The question that is spontaneous to ask is how it is possible to supply the necessary power to the activation of the SMA once the sail is in the space environment. Where the sail can be incorporated into a satellite, these could contain, in a CubeSat, a battery for the power supply, as already prepared for some prototypes launched in space such as the LightSail-1; instead, if the structure is designed for travel alone, then it could be equipped with solar cells for the generation of the energy required for the SMA activation. A similar solution was already adopted in the IKAROS project of the Japanese space agency JAXA.

Author Contributions: All authors have contributed equally to the work. All authors have read and agreed to the published version of the manuscript.

Funding: This research received no external funding.

Acknowledgments: The authors are grateful to Benedetto Iacovone and Piero Plini for the technical assistance in the experiments.

Conflicts of Interest: The authors declare no conflict of interest.

Nomenclature

m	mass (kg)
c	specific heat (320 J kg^{-1} K^{-1})
R	electric resistance (Ω)
ρ_t	Ni-Ti Resistivity (0.80 Ω mm^2/m)
I	electric current (A)
V	voltage (V)
v	volume
T_{amb}	ambient temperature (K)
σ	Boltzmann constant (5.67×10^{-8} W m^{-2} K^{-4})
h	convective heat transfer coefficient
ε	emissivity (0.17)
A	area (m^2)
A_f	austenite finish temperature (°C)
α	thermal diffusivity (derived, m^2 s^{-1})
ρ	density (NiTi 6.45, Al 2.7, Kapton 1.42, kg/dm^3)
$I_{o\,\beta}$	real solar irradiance (615 W/m^2)
SMA	shape memory alloy

References

1. Tsiolkowsky, K.E. Extension of Man into Outer Space. *Proc. Symp. Jet Propuls.* **1921**, *2*.
2. Tsuda, Y.; Mori, O.; Funase, R.; Sawada, H.; Yamamoto, T.; Saiki, T.; Endo, T.; Kawaguchi, J. Flight status of IKAROS deep space solar demonstrator. *Acta Astronaut.* **2011**, *69*, 833–840. [CrossRef]
3. Niccolai, L.; Anderlini, A.; Mengali, G.; Quarta, A.A. Impact of solar sail wind fluctuations on electric sail mission design. *Aerosp. Sci. Technol.* **2018**, *82*, 38–45. [CrossRef]
4. Block, J.; Straubel, M.; Wiedemann, M. Ultralight deployable booms for solar sails and other large gossamer structures in space. *Acta Astronaut.* **2011**, *68*, 984–992. [CrossRef]
5. Johnson, L.; Young, R.; Montgomery, E.; Alhorn, D. Status of solar sail technology within NASA. *Adv. Space Res.* **2011**, *48*, 1687–1694. [CrossRef]
6. Roman Kezera, Y.A. Thickness requirement for solar sail foils. *Acta Astronaut.* **2009**, *65*, 507–518.
7. Dalla Vedova, F.; Henrion, H.; Leipold, M.; Girot, T.; Vaudemont, R.; Belmonte, T.; Fleury, K.; Le Couls, O. The Solar Sail Materials (SSM) Project—Status of activities. *Adv. Space Res.* **2011**, *48*, 1922–1926. [CrossRef]

8. Fernandez, J.M.; Lappas, V.J.; Daton-Lovett, A.J. Completely stripped solar sail concept using bi-stable reeled composite booms. *Acta Astronaut.* **2011**, *69*, 78–85. [CrossRef]
9. Fu, B.; Eke, F. Further investigation of the body torques on a square solar sail due to the displacement of the sail attachment points. *Aerosp. Sci. Technol.* **2016**, *50*, 281–294. [CrossRef]
10. Mariner 10, NASA. National Space Science Data Center (NSSDC). Available online: https://nssdc.gsfc.nasa.gov/nmc/spacecraft/display.action?id=1973-085A (accessed on 20 November 2020).
11. Leipold, M.; Garner, C.E.; Freeland, R.; Herrmann, A.; Noca, M.; Pagel, G.; Sebolt, W.; Sprague, G.; Unckenbold, W. Odissee—A proposal for demonstration of a solar sail in earth orbit. *Acta Astronaut.* **1999**, *45*, 557–566. [CrossRef]
12. Mori, O.; Sawada, H.; Funase, R.; Endo, T.; Morimoto, M.; Yamamoto, T.; Tsuda, Y.; Kawakatsu, Y.; Kawaguchi, J. Development of first Solar Power Sail Demonstrator—Ikaros. In Proceedings of the 21st International Symposium on Space Flight Dynamics, Toulouse, France, 28 September–2 October 2009.
13. Johnson, L.; Whorton, M.; Heaton, A.; Pinson, R.; Laue, G.; Adams, C. NanoSail-D: A solar sail demonstration mission. *Acta Astronaut.* **2011**, *68*, 571–575. [CrossRef]
14. Nehrenz, M.; Diaz, A.; Svitek, T.; Biddy, C. Initial design and simulation of the LightSail-1 attitude determination and control system. In Proceedings of the 2nd International Symposium on Solar Sailing, New York, NY, USA, 20–22 July 2010; pp. 135–140.
15. MacNeal, R.H. *The Heliogyro-An Interplanetary Flying Machine*; NTRS—NASA Technical Reports Server: Santa Barbara, CA, USA, 1967.
16. Burton, R.L.; Coverstone, V.L.; Hargens-Rysanek, J.; Ertmer, K.; Botter, T.; Benavides, G.F.; Woo, B.; Carroll, D.L.; Gierow, P.; Farmer, G.; et al. Ultrasail—Ultralightweight solar sail concept. In Proceedings of the 41st AIAA/ASME/SAE/ASEE Joint Propulsion Conference, Tucson, AZ, USA, 10–13 July 2005.
17. Costanza, G.; Tata, M.E. Design and characterization of a small-scale solar sail deployed by NiTi Shape Memory Actuators. *Procedia Struct. Integr.* **2016**, *2*, 1451–1456. [CrossRef]
18. Costanza, G.; Tata, M.E. A novel methodology for solar sail opening employing shape memory alloy elements. *J. Intell. Mater. Syst. Struct.* **2018**, *29*, 1793–1798. [CrossRef]
19. Costanza, G.; Leoncini, G.; Quadrini, F.; Tata, M.E. Design and characterization of a small-scale solar sail prototype by integrating NiTi SMA and carbon fibre composite. *Adv. Mater. Sci. Eng.* **2017**, *2017*, 8467971. [CrossRef]
20. Otsuka, K.; Ren, X. Physical metallurgy of Ti-Ni-based shape memory alloys. *Progr. Mater. Sci.* **2005**, *50*, 511–678. [CrossRef]
21. Costanza, G.; Tata, M.E.; Libertini, R. Effect of temperature on the mechanical behavior of Ni-Ti Shape Memory Sheets. In Proceedings of the TMS2016 145th Annual Meeting Supplemental Proceedings, Nashville, TN, USA, 14–18 February 2016; pp. 433–439.
22. Costanza, G.; Paoloni, S.; Tata, M.E. IR thermography and resistivity investigations on Ni-Ti shape memory alloys. *Key Eng. Mater.* **2014**, *605*, 23–26. [CrossRef]
23. Costanza, G.; Tata, M.E.; Calisti, C. Nitinol one-way shape memory springs: Thermomechanical characterization and actuator design. *Sens. Actuators A Phys.* **2010**, *157*, 113–117. [CrossRef]
24. Bovesecchi, G.; Corasaniti, S.; Costanza, G.; Tata, M.E. A Novel Self-Deployable Solar Sail System Activated by Shape Memory Alloys. *Aerospace* **2019**, *6*, 78. [CrossRef]
25. Boschetto, A.; Bottini, L.; Costanza, G.; Tata, M.E. Shape-memory activated self-deployable solar sails: Small-scale prototypes manufacturing and planarity analysis by 3D laser scanner. *Actuators* **2019**, *8*, 38. [CrossRef]
26. Costanza, G.; Tata, M.E. Shape memory alloys for aerospace, recent developments, and new applications: A short review. *Materials* **2020**, *13*, 1856. [CrossRef] [PubMed]